Full-Duplex Massive MIMO Self-Interference Suppression Based on Beamforming

ZHANG Boyu, ZHANG Ling, LI Zijing, SHEN Ying
(University of Electronic Science and Technology of China, Chengdu 611731, China)

DOI: 10.12142/ZTECOM.202504011
https://kns.cnki.net/kcms/detail/34.1294.TN.20251107.1127.004.html, published online November 7, 2025
Manuscript received: 2024-04-10

Abstract: The complexities of hardware and signal processing make it especially challenging to develop self-interference cancellation (SIC) techniques for full-duplex (FD) massive multiple-input-multiple-output (MIMO) systems. This paper examines an FD massive MIMO system featuring multi-stream transmission. Specifically, it adopts an architecture where a single transmit or receive radio frequency (RF) channel is connected to three antennas in the same polarization direction, effectively reducing the number of transmit and receive RF channels by half. The SoftNull algorithm serves as the primary method for SI suppression, leveraging digital precoding during transmission. Additionally, this study outlines a design strategy to enhance SIC in the proposed system. Simulation results highlight the efficacy of the SoftNull algorithm, which achieves a remarkable total SIC of up to 64 dB. Furthermore, combined with measures such as antenna isolation and increased transceiver array spacing, the resulting sum rate can be twice that of a half-duplex system.

Keywords: full-duplex; massive MIMO; self-interference; beamforming; precoding

Citation (Format 1): ZHANG B Y, ZHANG L, LI Z J, et al. Full-duplex massive MIMO self-interference suppression based on beamforming [J]. ZTE Communications, 2025, 23(4): 97 - 109. DOI: 10.12142/ZTECOM.202504011
Citation (Format 2): B. Y. Zhang, L. Zhang, Z. J. Li, et al., "Full-duplex massive MIMO self-interference suppression based on beamforming," *ZTE Communications*, vol. 23, no. 4, pp. 97 - 109, Sept. 2025. doi: 10.12142/ZTECOM.202504011.

1 Introduction

In recent years, the full-duplex (FD) and massive multiple-input-multiple-output (MIMO) technologies have emerged as key research focuses in wireless communications[1-4]. As a key technology of 5G, FD technology allows radios to simultaneously transmit and receive in the same frequency band, which theoretically doubles the spectrum utilization rate compared with the traditional duplex system[5-6]. As another key technology of 5G, massive MIMO can improve the spectral efficiency and reliability of a system by equipping a large number of antennas[7-11]. In 5G wireless technology implementations, the combination of various technologies has become a trend[12-13]. Both FD and massive MIMO technologies have the characteristics of high spectral efficiency, so the combination of the two can further improve the spectral efficiency.

In FD communications, signals sent by the wireless transceiver bring self-interference (SI) to its reception[14]. Strong SI signals may overwhelm useful information and cause errors in the received data. For a low noise amplifier (LNA) at the receive radio frequency (RF) channel, it may also exceed the dynamic range of its input, bringing harm to receiver hardware. Therefore, SI cancellation (SIC) is critical for realizing FD communications[15]. For FD massive MIMO systems, each receive antenna will be interfered by multiple transmit antennas, and SIC becomes more challenging as the number of antennas increases.

Numerous SIC algorithms have been proposed to solve the issues of strong SI in FD massive MIMO systems. In Ref. [16], an adaptive filter structure with analog least mean square (ALMS) loops is proposed, which only realizes SIC in the analog domain. Although the number of taps used is greatly reduced, additional taps are still needed and the hardware complexity is high. To further reduce hardware complexity, some studies have put forward a combination of digital beamforming and analog SIC to reduce SI. For FD MIMO systems, Ref. [17] introduces a novel analog SI canceller which utilizes the flexible signal routing of Mux/DeMux to reduce the taps' number in the analog SI canceller. It also develops a novel optimization framework for the joint design of the analog canceller and TX/RX digital beamforming parameters. The burden of SIC is shared between digital beamforming and analog SI cancellers, which greatly reduces the hardware complexity. In Ref. [18], a joint design framework of TX-RX beamforming and SIC scheme based on the minimum mean square error (MMSE) is introduced to realize SIC under the constraint of analog canceller tap limits. Hybrid precoding/combining (HPC) techniques have also been discussed recently. A novel angular-

based joint hybrid precoding/combining technique is explored in Ref. [19] for FD massive MIMO systems, combining transmit/receive RF beamformers and receiver combiners to achieve SIC. In Ref. [20], the authors propose a hybrid beamforming design for FD massive MIMO systems, which jointly designs the transmit RF beamformer, the precoder, and the combiner to suppress SI. However, all the HPC-based SIC technologies rely on RF beamformers, resulting in an increased signal processing complexity. In Ref. [21], a SIC algorithm, SoftNull, is proposed that uses only transmit digital precoding. It requires no additional analog SI cancellers, nor does it need to be designed with an RF beamformer, which drastically reduces both hardware and signal processing complexity.

Focusing on the multi-stream FD massive MIMO communication system[19], this paper studies a SIC method based on a 3D geometry-based millimeter wave (mmWave) channel model. In the proposed system model, the transmit and receive antennas are all ±45° polarized, and one transmit or receive RF channel is connected with three transmit or receive antennas in the same polarization direction. The number of required RF channels is reduced by half, greatly reducing the volume and cost. At the same time, the 3D geometry-based mmWave channel model is used to model the intended and the SI channels. In view of the above system architecture, the SoftNull algorithm based only on transmit digital precoding is selected to realize SIC, which requires neither additional hardware structure nor RF beamformer processing. Specifically, the proposed method takes advantage of the high degree of freedom provided by large antenna arrays to split the conventional transmit digital precoding matrix into two submatrices: one for traditional digital precoding and the other for SIC. In this way, it can minimize the total SI power while preserving a certain degree of freedom for traditional digital precoding.

In addition, concerning the proposed system architecture, the method of improving SIC ability using the SoftNull algorithm is analyzed theoretically. The analysis results indicate that the ability of SIC can be enhanced by measures such as designing polarization isolation degree between transceiver arrays with different polarization directions, changing the array layout, and increasing the size of transmit/receive uniform rectangular arrays (URA). Simulation results demonstrate that the SoftNull algorithm can achieve up to 64 dB of SIC under the proposed system architecture. To achieve higher system performance, joint antenna isolation and the SoftNull algorithm are proposed. Simulation verifies that when the antenna isolation is increased to 50 dB, the sum rate is 1.7 times higher than that of the standalone SoftNull algorithm and twice as high as the half-duplex algorithm at low signal-to-noise ratios (SNRs). Furthermore, system performance can be further improved by increasing the size of transmit/receive URAs. Simulation results show that the sum rate of the SoftNull algorithm can be improved by up to 54% compared with the same antenna isolation when the size of the transmit/receive URA is increased to 5 wavelengths, and it remains nearly double that of the half-duplex state at high SNRs.

The rest of this article is organized as follows. Section 2 presents the system model and channel model. In Section 3, a SoftNull algorithm is introduced and the method of enhancing the SIC effect is analyzed theoretically. Section 4 demonstrates the effectiveness of the algorithm under the proposed system architecture, and simulations are carried out by further improving the system performance. Finally, Section 5 concludes this paper.

2 System Model and Channel Model

We consider a system model for the FD massive MIMO system, where the base station (BS) has a precoder (with a precoding matrix $\boldsymbol{V}_{\mathrm{BS}} \in \boldsymbol{C}^{N_{\mathrm{RF},t} \times K_{\mathrm{Down}}}$) and a combiner (with a matrix $\boldsymbol{U}_{\mathrm{BS}} \in \boldsymbol{C}^{K_{\mathrm{Up}} \times N_{\mathrm{RF},r}}$), as shown in Fig. 1.

The transmitter and the receiver of BS, which operate in a full-duplex mode, are equipped with N_t and N_r antennas, and by $N_{\mathrm{RF},t}$ and $N_{\mathrm{RF},r}$ RF chains, respectively. Each transmit or receive RF chain is attached to three dedicated transmit or receive antenna elements via a power combiner or power divider, where $N_{\mathrm{RF},t} = N_t/3$, $N_{\mathrm{RF},r} = N_r/3$. Each power divider is applied to make three copies of the signals processed at a TX RF chain before these signals enter the TX antenna elements. Similarly, each power combiner is used to add the signals received by three RX antenna elements before these signals enter the RX RF chain. The proposed system decreases the hardware cost and complexity of traditional FD massive MIMO systems, due to the number of RF channels being reduced from $N_t + N_r$ to $N_{RF,t} + N_{RF,r} = (N_t + N_r)/3$. The half-duplex (HD) single-antenna users in the system are divided into K_{Up} users transmitting in the uplink mode and K_{Down} users receiving in the downlink mode, which are denoted as nodes "Up" and nodes "Down", respectively, where $K_{\mathrm{Up}}, K_{\mathrm{Down}} \leqslant \{N_{\mathrm{RF},t}, N_{\mathrm{RF},r}\}$.

The transmitter of BS employs both traditional digital precoding and SI suppression using the matrices $\boldsymbol{B}$ and $\boldsymbol{A}$ of size $f_{\mathrm{D}} \times K_{\mathrm{Down}}$ and $N_{\mathrm{RF},t} \times f_{\mathrm{D}}$ to process the baseband signal $\boldsymbol{S}_{\mathrm{BS},t} \in \boldsymbol{C}^{K_{\mathrm{Down}} \times 1}$ in the frequency domain, respectively. The beamformed signal undergoes $N_{\mathrm{RF},t}$ transmission RF channels and the N_t transmission antenna, and this generates as a downlink transmission signal S. f_D represents the degree of freedom available for traditional digital precoding, that is, the degree of freedom allocated for downlink traditional beamforming. Additionally, it should be guaranteed that $K_{\mathrm{Down}} \leqslant f_D \leqslant N_{\mathrm{RF},t}$. The downlink transmission signal can be mathematically expressed as:

$$\boldsymbol{x}_{\mathrm{BS},t} = \boldsymbol{C}_t \boldsymbol{F}^H \boldsymbol{V}_{\mathrm{BS}} \boldsymbol{S}_{\mathrm{BS},t} \tag{1},$$

where $\boldsymbol{V}_{\mathrm{BS}} = \mathbf{AB} \in \boldsymbol{C}^{N_{\mathrm{RF},t} \times K_{\mathrm{Down}}}$ is the equivalent transmission digital precoding matrix, and $\boldsymbol{F} \in \boldsymbol{C}^{N_{\mathrm{RF},t} \times N_{\mathrm{RF},t}}$ denotes the fast Fourier transform matrix. The elements $[\boldsymbol{F}]_{m,k}$ with $m, k =$

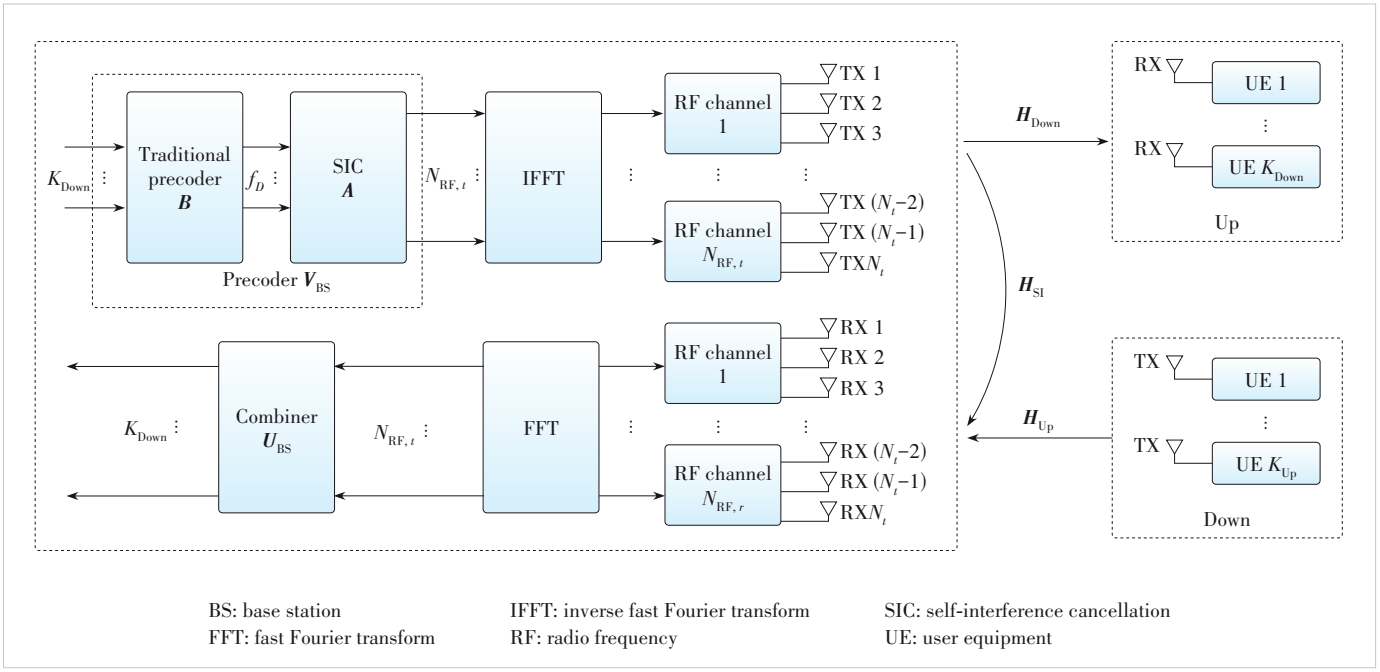

Figure 1. FD massive MIMO communication system with multi-stream transmission

0,1,⋯, $N-1$ take $e^{-j2\pi mk/N}/\sqrt{N}$. $\boldsymbol{C}_t \in \boldsymbol{C}^{N_t \times N_{RF,t}}$ represents the matrix from the transmitting RF channel to the TX antenna on the BS side, which is obtained as:

$$\boldsymbol{C}_t = \frac{1}{3}\boldsymbol{E}_{N_{RF,t}} \otimes \left[\boldsymbol{E}_{N_{t,y}}, \quad \boldsymbol{E}_{N_{t,y}}, \quad \boldsymbol{E}_{N_{t,y}}\right]^{\mathrm{T}} \tag{2},$$

where $\boldsymbol{E}_N$ denotes the n-th order unit array.

As shown in Fig. 1, when the BS transmits data to the node Down and the node Up transmits data to the BS, the corresponding intended channel matrix between them is denoted as $\boldsymbol{H}_{Down} \in \boldsymbol{C}^{K_{Down} \times N_t}$ and $\boldsymbol{H}_{Up} \in \boldsymbol{C}^{N_r \times K_{Up}}$, respectively. Moreover, $\boldsymbol{H}_{SI} \in \boldsymbol{C}^{N_r \times N_t}$ represents the SI channel at the BS due to the FD transmission. It is assumed that there is no interference between the nodes Down and Up. We model both the intended channel and the SI channel in the following content.

Fig. 2 illustrates the application scenario, where the transmitter and receiver employ a uniform rectangular array (URA) with ±45° polarization on the BS side. For convenience, we use polarization 1 and 2 to denote polarization +45° and −45°. The transmit or receive antennas with different polarizations are placed in the same position. The number of transmit or receive antennas with polarization k is $N_u^k = N_{u,x} \times N_{u,y}, u \in \{t, r\}, k \in \{1, 2\}$, where $u \in \{t, r\}$ represents either the transmitter side for $u = t$ or the receiver side for $u = r$. Here, $N_{u,x}$ and $N_{u,y}$ represent the antennas along the x-axis and the y-axis, respectively, where $N_t^1 = N_t^2$ and $N_r^1 = N_r^2$.

The transmit and receive URAs of BS located in the x-o-y plane are placed next to each other, where d_1 represents the distance between the transmit and receive URAs along the x-axis.

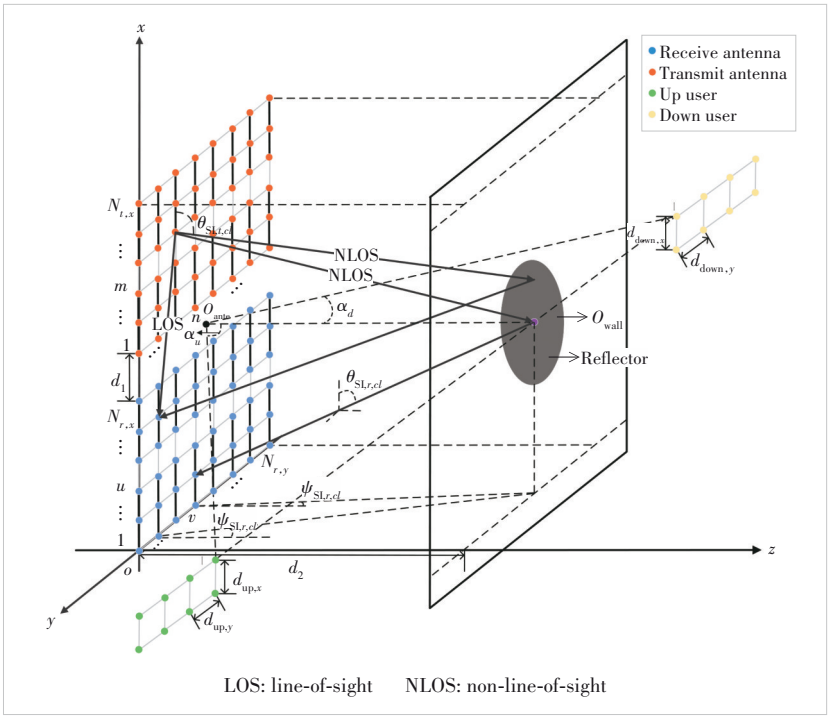

Figure 2. Application scenarios of FD massive MIMO system

Consider a wall parallel to the transmit and receive URAs, with a distance d_2 between them. The wall's center point o_{ante} is at the same height as the center point o_{ante} of transmit and receive URAs. Both the nodes Down and $\boldsymbol{V}_{\text{BS}}$ are located on the plane of the wall, which are respectively located on the positive y-axis and the negative y-axis. Uplink user 1 and downlink user 1 are at the same height as o_{ante} at the angle of α_u and α_d.

We assume that there are $K_{\text{Up},x}$ and $K_{\text{Up},y}$ uplink users regularly arranged along the negative x-axis and the positive y-axis with an interval of $d_{\text{Up},x}$ and $d_{\text{Up},y}$. Similarly, there are $K_{\text{Down},x}$ and $N_{\text{RF},t}$ uplink users regularly arranged along the negative x-axis and the positive y-axis with the intervals of $d_{\text{Down},x}$ and $d_{\text{Down},x}$, where $K_{\text{Up}} = K_{\text{Up},x} \times K_{\text{Up},y}$, $\boldsymbol{H}_{\text{equ}} = \boldsymbol{H}_{\text{Down,equ}}\boldsymbol{A}$.

Fig. 3 shows the structure of transmit and receive URAs, where each transmit or receive RF chain is connected to three dedicated transmit or receive antenna elements in the same polarization. $N^k_{\text{RF},u}, u \in \{t,r\}, k \in \{1,2\}$ indicates the number of transmit or receive RF chains attached to the antenna with polarization k, where $N^1_{\text{RF},t} = N^2_{\text{RF},t}$ and $N^1_{\text{RF},r} = N^2_{\text{RF},r}$.

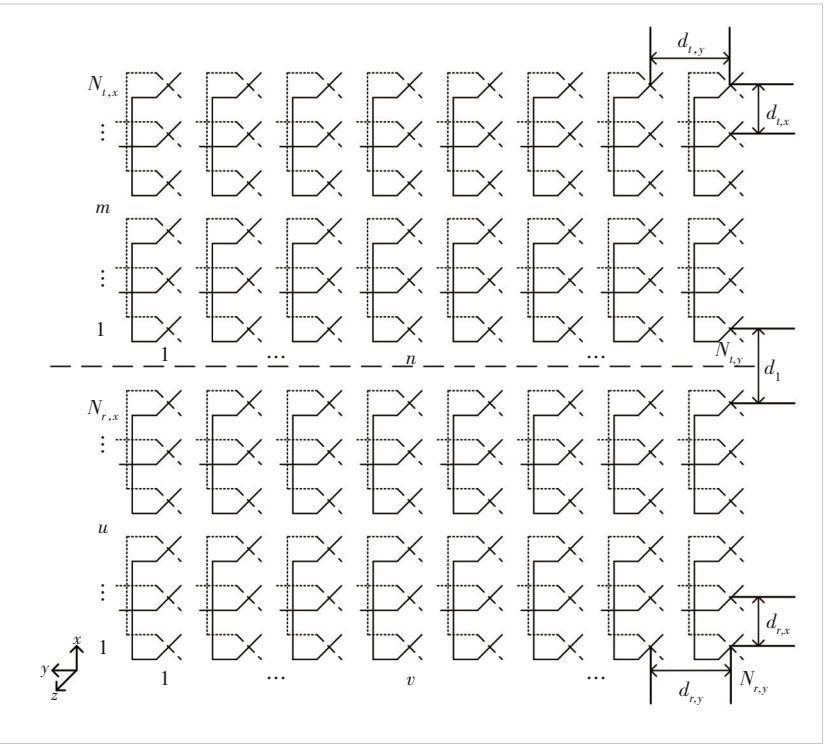

Figure 3. Base station transceiver's uniform rectangular array structure

$N_{t,x}$ and $N_{t,y}$ transmit antenna elements in the same polarization are arranged with equal intervals $d_{t,x}$ and $d_{t,y}$ along the positive x-axis and the negative y-axis, respectively. Similarly, $N_{r,x}$ and $N_{r,y}$ transmit antenna elements in the same polarization are arranged with equal intervals $d_{t,x}$ and $d_{t,y}$ along the positive x-axis and the negative y-axis, respectively.

Intended channels are modeled using the 3D geometry-based mmWave channel model and the system application scenario. We assume that the intended channels contain C_i scattering clusters and $L_{i,c}$ paths in the c-th cluster with $c = 1,2,\cdots,C_i$. There are $L_i = \sum_{c=1}^{C_i} L_{i,c}$ paths between the transmitter and receiver in total. The intended channel matrix is derived as:

$$\boldsymbol{H}_i = \sum_{c=1}^{C_i}\sum_{l=1}^{L_{i,c}} \tau_{i,c_l}^{-\eta} g_{i,c_l} \boldsymbol{\phi}_{r,j}\left(\boldsymbol{\gamma}_{r,c_l}^{(x)},\boldsymbol{\gamma}_{r,c_l}^{(y)}\right)\boldsymbol{\phi}_{t,i}^{H}\left(\boldsymbol{\gamma}_{t,c_l}^{(x)},\boldsymbol{\gamma}_{t,c_l}^{(y)}\right) = \boldsymbol{\Phi}_{r,j}\boldsymbol{G}_i\boldsymbol{\Phi}_{t,i} \tag{3}$$

where $\boldsymbol{H}_i \in C^{R\times T}$ $(R,T) \in \left\{\left(K_{\text{Down}},N_t\right),\left(N_r,K_{\text{Up}}\right)\right\}$; j and i are the receive and transmit nodes of the intended channel, satisfying $(j,i) \in \left\{(\text{Down},\text{BS}),(\text{BS},\text{Up})\right\}$. When $(j,i) = (\text{Down},\text{BS})$, there is $(R,T) = \left(K_{\text{Down}},N_t\right)$. When $(j,i) = (\text{BS},\text{Up})$, there is $(R,T) = \left(N_r,K_{\text{Up}}\right)$. $\boldsymbol{G}_i = \text{diag}\left(\tau_{i,1}^{-\eta}g_{i,1},\cdots,\tau_{i,L_i}^{-\eta}g_{i,L_i}\right) \in C^{L_i\times L_i}$ represents the diagonal path gain matrix, τ_{i,c_l} and $g_{i,l}\sim CN\left(0,1/L_i\right)$ denote the distance and complex path gain of the l-th path in the c-th cluster, respectively. η is the path loss exponent. $\boldsymbol{\Phi}_{r,j} \in C^{R\times L_i}$ and $\boldsymbol{\Phi}_{t,i} \in C^{L_i\times T}$ respectively represent the receive and transmit phase response matrices of intended channels, which is given by:

$$\boldsymbol{\Phi}_{r,j} = \begin{bmatrix} \boldsymbol{\phi}_{r,j}^{H}\left(\boldsymbol{\gamma}_{r,1}^{(x)},\boldsymbol{\gamma}_{r,1}^{(y)}\right) \\ \vdots \\ \boldsymbol{\phi}_{r,j}^{H}\left(\boldsymbol{\gamma}_{r,L_i}^{(x)},\boldsymbol{\gamma}_{r,L_i}^{(y)}\right) \end{bmatrix}^{H} \tag{4}$$

$$\boldsymbol{\Phi}_{t,i} = \begin{bmatrix} \boldsymbol{\phi}_{t,i}^{H}\left(\boldsymbol{\gamma}_{t,1}^{(x)},\boldsymbol{\gamma}_{t,1}^{(y)}\right) \\ \vdots \\ \boldsymbol{\phi}_{t,i}^{H}\left(\boldsymbol{\gamma}_{t,L_i}^{(x)},\boldsymbol{\gamma}_{t,L_i}^{(y)}\right) \end{bmatrix} \tag{5}$$

where $\boldsymbol{\phi}_{u,i}\left(\boldsymbol{\gamma}_{u,c_l}^{(x)},\boldsymbol{\gamma}_{u,c_l}^{(y)}\right) \in C^{U\times 1},(U,u) \in \left\{(R,r),(T,t)\right\}$ denotes the phase response vector of the l-th path in the c-th cluster, which can be expressed as:

$$\boldsymbol{\phi}_{u,i}\left(\boldsymbol{\gamma}_x,\boldsymbol{\gamma}_y\right) = \left[1,\quad e^{j2\pi d_{u,x}\gamma_x},\quad \cdots,\quad e^{j2\pi d_{u,x}\left(N_{u,x}-1\right)\gamma_x}\right]^{\text{T}} \otimes \left[1,\quad e^{j2\pi d_{u,y}\gamma_y},\quad \cdots,\quad e^{j2\pi d_{u,y}\left(N_{u,y}-1\right)\gamma_y}\right]^{\text{T}} \tag{6}$$

$\gamma_{r,c_l}^{(x)}$ and $\gamma_{r,c_l}^{(y)}$ include the elevation angle-of-arrival (AoA) and azimuth AoA information of the receive antenna of the l-th path in the c-th cluster at node j, which can be written as follows:

$$\gamma_{r,c_l}^{(x)} = \sin(\theta_{r,c_l})\cos(\psi_{r,c_l}) \tag{7},$$

$$\gamma_{r,c_l}^{(y)} = \sin(\theta_{r,c_l})\sin(\psi_{r,c_l}) \tag{8}.$$

The elevation AoA θ_{r,c_l} and azimuth AoA ψ_{r,c_l} are the angle between the path and the positive x-axis and that between the projection of the path on the y-o-z plane and the positive z-axis, respectively. $\gamma_{t,c_l}^{(x)}$ and $\gamma_{t,c_l}^{(y)}$ indicate the elevation angles of departure (AoD) and azimuth AoD of the transmit antenna of the l-th path in the c-th cluster at the node i, and can be mathematically expressed as:

$$\gamma_{t,c_l}^{(x)} = \sin(\theta_{t,c_l})\cos(\psi_{t,c_l}) \tag{9},$$

$$\gamma_{t,c_l}^{(y)} = \sin(\theta_{t,c_l})\sin(\psi_{t,c_l}) \tag{10},$$

where θ_{t,c_l} and ψ_{t,c_l} respectively represent the elevation AoD and azimuth AoD of the l-th path in the c-th cluster.

According to the application scenario in Fig. 2, SI channels can be divided into the residual near-field SI channel $\boldsymbol{H}_{\mathrm{LoS}} \in \boldsymbol{C}^{N_r \times N_t}$ and the far-field SI channel $\boldsymbol{H}_{\mathrm{NLoS},i} \in \boldsymbol{C}^{N_r \times N_t}$ after antenna isolation, which can be obtained as:

$$\boldsymbol{H}_{\mathrm{SI}} = \boldsymbol{H}_{\mathrm{LoS}} + \boldsymbol{H}_{\mathrm{NLoS}} \tag{11}.$$

With the transmit and receive URA structure in Fig. 3, $\boldsymbol{H}_{\mathrm{LoS}}$ is derived as:

$$\boldsymbol{H}_{\mathrm{LoS}} = \begin{bmatrix} \boldsymbol{H}_{\mathrm{LoS}}^{11} & \boldsymbol{H}_{\mathrm{LoS}}^{12} \\ \boldsymbol{H}_{\mathrm{LoS}}^{21} & \boldsymbol{H}_{\mathrm{LoS}}^{22} \end{bmatrix} \tag{12},$$

where $\boldsymbol{H}_{\mathrm{LoS}}^{gk} \in \boldsymbol{C}^{N_r^g \times N_t^k}, g,k \in \{1,2\}$ represents the residual near-field SI channel between the element with polarization g of receive array and the element with polarization k of the transmit array. We assume that the antenna polarization isolation between each transceiver array element is $\boldsymbol{P}_{\mathrm{XPI,dB}} = -10\log 10(\boldsymbol{K}) \in \boldsymbol{C}^{N_r^g \times N_t^k}, g \neq k$. Eq. (12) is equivalent to:

$$\boldsymbol{H}_{\mathrm{LoS}} = \begin{bmatrix} \boldsymbol{H}_{\mathrm{LoS}}^{11} & \boldsymbol{K} \odot \boldsymbol{H}_{\mathrm{LoS}}^{11} \\ \boldsymbol{K} \odot \boldsymbol{H}_{\mathrm{LoS}}^{11} & \boldsymbol{H}_{\mathrm{LoS}}^{11} \end{bmatrix} \tag{13}.$$

The residual near-field SI channel $\boldsymbol{H}_{\mathrm{LoS}}^{11}$ between transmit and receive array elements with polarization 1 is detailed in the following. The element of the $[(u-1)N_{r,y}+v]$ row and $[(m-1)N_{t,y}+n]$ column of $\boldsymbol{H}_{\mathrm{LoS}}^{11}$, which is the channel between the (m,n)-th transmitter and (u,v)-th receiver in Fig. 3, can be given by

$$\boldsymbol{H}_{\mathrm{LoS}}^{11}([(u-1)N_{r,y}+v],[(m-1)N_{t,y}+n]) = \frac{\kappa_1}{\Delta_{(m,n)\to(u,v)}} \mathrm{e}^{-j2\pi\Delta_{(m,n)\to(u,v)}} \tag{14},$$

where κ_1 is a constant satisfying $10\log\{\mathrm{E}[\|\boldsymbol{H}_{\mathrm{LoS}}^{11}\|_F^2]\} = -P_{\mathrm{IS,dB}}$; $P_{\mathrm{IS,dB}}$ is the antenna isolation, and $\Delta_{(m,n)\to(u,v)}$ is the distance from the (m,n)-th transmitter to the (u,v)-th receiver. $\Delta_{(m,n)\to(u,v)}$ is defined as follows:

$$\Delta_{(m,n)\to(u,v)} = \sqrt{[(m-1)d_{t,x}+(u-1)d_{r,x}+D_1]^2+(nd_{t,y}-vd_{r,y})^2} \tag{15}.$$

Similarly, the far-field SI channel can be obtained as

$$\boldsymbol{H}_{\mathrm{NLoS}} = \begin{bmatrix} \boldsymbol{H}_{\mathrm{NLoS}}^{11} & \boldsymbol{K} \odot \boldsymbol{H}_{\mathrm{NLoS}}^{11} \\ \boldsymbol{K} \odot \boldsymbol{H}_{\mathrm{NLoS}}^{11} & \boldsymbol{H}_{\mathrm{NLoS}}^{11} \end{bmatrix} \tag{16},$$

where $\boldsymbol{H}_{\mathrm{NLoS}}^{11} \in \boldsymbol{C}^{N_r^1 \times N_t^1}$ represents the far-field SI channel between the receive and transmit array elements with polarization 1. We utilize the 3D geometry-based mmWave channel to model $\boldsymbol{H}_{\mathrm{NLoS}}^{11}$. Suppose there are C_{SI} scattering clusters, and c cluster contains $L_{\mathrm{SI},c}$ non-line-of-sight (NLOS) paths with $c = 1,2,\cdots,C_{\mathrm{SI}}$. In total, there are $L_{\mathrm{SI}} = \sum_{c=1}^{C_{\mathrm{SI}}} L_{\mathrm{SI},c}$ paths between the transmitter and receiver. According to Eq. (3), it can be mathematically expressed as

$$\boldsymbol{H}_{\mathrm{NLoS}}^{11} = \boldsymbol{\Phi}_{\mathrm{SI},r}\boldsymbol{G}_{\mathrm{SI}}\boldsymbol{\Phi}_{\mathrm{SI},t} \tag{17},$$

where $\boldsymbol{G}_{\mathrm{SI}} = \mathrm{diag}\left(\tau_{\mathrm{SI},1}^{-\eta} g_{\mathrm{SI},1},\cdots,\tau_{\mathrm{SI},L_{\mathrm{SI}}}^{-\eta} g_{\mathrm{SI},L_{\mathrm{SI}}}\right) \in C^{L_{\mathrm{SI}} \times L_{\mathrm{SI}}}$ denotes the diagonal path gain matrix, τ_{SI,c_l} and $g_{\mathrm{SI},l} \sim CN\left(0,1/L_{\mathrm{SI}}\right)$ respectively represent the distance and complex path gain of the l-th path in the c-th cluster. $\boldsymbol{\Phi}_{\mathrm{SI},r} \in C^{N_r \times L_{\mathrm{SI}}}$ and $\boldsymbol{\Phi}_{\mathrm{SI},t} \in C^{L_{\mathrm{SI}} \times N_t}$ denote the receive and the transmit phase response matrices of the far-field SI channel, respectively. We assume $\theta_{\mathrm{SI},r,c_l}$ and ψ_{SI,r,c_l} indicate elevation AoA and azimuth AoA of the l-th NLOS path in the c-th cluster. $\theta_{\mathrm{SI},t,c_l}$ and ψ_{SI,t,c_l} respectively represent elevation AoD and azimuth AoD of the l-th NLOS path in the c-th cluster. Therefore, Eq. (11) is equivalent to:

$$\boldsymbol{H}_{\mathrm{SI}} = \begin{bmatrix} \boldsymbol{H}_{\mathrm{SI}}^{11} & \boldsymbol{K} \odot \boldsymbol{H}_{\mathrm{SI}}^{11} \\ \boldsymbol{K} \odot \boldsymbol{H}_{\mathrm{SI}}^{11} & \boldsymbol{H}_{\mathrm{SI}}^{11} \end{bmatrix} \tag{18},$$

where $\boldsymbol{H}_{\mathrm{SI}}^{11} = \boldsymbol{H}_{\mathrm{LoS}}^{11} + \boldsymbol{H}_{\mathrm{NLoS}}^{11} \in \boldsymbol{C}^{N_r^1 \times N_t^1}$ is the SI channel between transmit and receive array elements with polarization 1.

In the downlink transmission, the received signals $\boldsymbol{y}_{\mathrm{UE},r} \in \boldsymbol{C}^{K_{\mathrm{Down}} \times 1}$ at nodes Down are obtained as:

$$\boldsymbol{y}_{\mathrm{UE},r} = \boldsymbol{H}_{\mathrm{Down}}\boldsymbol{x}_{\mathrm{BS},t} + \boldsymbol{n}_{\mathrm{UE}} \tag{19},$$

where $\mathbf{n}_{\mathrm{UE}} \sim CN\left(0,\sigma_{\mathrm{UE}}^2\mathbf{I}_{K_{\mathrm{Down}}}\right) \in \mathbf{C}^{K_{\mathrm{Down}}\times 1}$ denotes the additive white Gaussian noise (AWGN) vector at nodes Down.

The BS simultaneously transmits messages to nodes Down in the downlink and receives information from nodes Up in the uplink in the FD mode. Hence, the received signal vector $\boldsymbol{y}_{\mathrm{BS},r} \in \boldsymbol{C}^{N_r\times 1}$ at the receiver of BS includes the downlink transmission signals $\boldsymbol{x}_{\mathrm{BS},t}$ through the SI channels and the uplink transmission signals $\boldsymbol{x}_{\mathrm{UE},t} \in \boldsymbol{C}^{K_{\mathrm{Up}}\times 1}$ through the uplink channel. It can be expressed as:

$$\boldsymbol{y}_{\mathrm{BS},r} = \boldsymbol{H}_{\mathrm{Up}}\boldsymbol{x}_{\mathrm{UE},t} + \boldsymbol{H}_{\mathrm{SI}}\boldsymbol{x}_{\mathrm{BS},t} + \boldsymbol{n}_{\mathrm{BS}} \tag{20},$$

where $\boldsymbol{n}_{\mathrm{BS}} \sim CN\left(0,\sigma_{\mathrm{BS}}^2\boldsymbol{I}_{N_r}\right) \in \boldsymbol{C}^{N_r\times 1}$ is the AWGN vector at the BS receiver.

Upon signal $\boldsymbol{y}_{\mathrm{BS},r}$ reception at the BS, RX RF chains first process signals received at the RX antenna elements. Assuming that output signals of the RX RF chains are processed in the frequency domain by the received digital combiner $\boldsymbol{U}_{\mathrm{BS}} \in \boldsymbol{C}^{K_{\mathrm{Up}}\times N_{\mathrm{RF},r}}$, vector $\boldsymbol{S}_{\mathrm{BS},r} \in \boldsymbol{C}^{K_{\mathrm{Up}}\times 1}$ is derived as:

$$\boldsymbol{S}_{\mathrm{BS},r} = \boldsymbol{U}_{\mathrm{BS}}\boldsymbol{F}\boldsymbol{C}_r\boldsymbol{y}_{\mathrm{BS},r} \tag{21},$$

where $\boldsymbol{C}_r = \frac{1}{3}\boldsymbol{E}_{N_{\mathrm{RF},r}} \otimes \left[\boldsymbol{E}_{N_{r,y}},\ \boldsymbol{E}_{N_{r,y}},\ \boldsymbol{E}_{N_{r,y}}\right] \in \boldsymbol{C}^{N_{\mathrm{RF},r}\times N_r}$ is the equivalent matrix from the receive antenna to the receive RF channel at the BS. We utilize $\boldsymbol{H}_{\mathrm{Down,equ}} = \boldsymbol{H}_{\mathrm{Down}}\boldsymbol{C}_t \in \boldsymbol{C}^{K_{\mathrm{Down}}\times N_{\mathrm{RF},t}}$ and $\boldsymbol{H}_{\mathrm{Up,equ}} = \boldsymbol{C}_r\boldsymbol{H}_{\mathrm{Up}} \in \boldsymbol{C}^{N_{\mathrm{RF},r}\times K_{\mathrm{Up}}}$ to represent the equivalent of downlink channel from the TX RF channel at the BS to nodes Down and the uplink channel from nodes Up to the RX RF channel at the BS, respectively. The equivalent SI channel from the TX RF channel to the RX RF channel at the BS is noted as $\boldsymbol{H}_{\mathrm{SI,equ}} = \boldsymbol{C}_r\boldsymbol{H}_{\mathrm{SI}}\boldsymbol{C}_t \in \boldsymbol{C}^{N_{\mathrm{RF},r}\times N_{\mathrm{RF},t}}$. Eq. (19) is derived as:

$$\boldsymbol{y}_{\mathrm{UE},r} = \boldsymbol{H}_{\mathrm{Down,equ}}\boldsymbol{F}^{\mathrm{H}}\boldsymbol{V}_{\mathrm{BS}}\boldsymbol{S}_{\mathrm{BS},t} + \boldsymbol{n}_{\mathrm{UE}} \tag{22}.$$

Eq. (21) is obtained as:

$$\mathrm{S}_{\mathrm{BS},r} = \boldsymbol{U}_{\mathrm{BS}}\boldsymbol{F}\boldsymbol{H}_{\mathrm{Up,equ}}\boldsymbol{x}_{\mathrm{UE},t} + \boldsymbol{U}_{\mathrm{BS}}\boldsymbol{F}\boldsymbol{H}_{\mathrm{SI,equ}}\boldsymbol{F}^{\mathrm{H}}\boldsymbol{V}_{\mathrm{BS}}\boldsymbol{S}_{\mathrm{BS},t} + \boldsymbol{U}_{\mathrm{BS}}\boldsymbol{F}\boldsymbol{C}_r\boldsymbol{n}_{\mathrm{BS}} \tag{23}.$$

3 SoftNull Algorithm for FD Massive MIMO System

To achieve SIC, the SoftNull algorithm based on the transmit digital precoding matrix is adopted in this paper. The algorithm has two primary design objectives for the transmit digital precoding matrix: ensuring the useful signal power and minimizing the total SI signal power. By splitting the transmit digital precoding matrix $\boldsymbol{V}_{\mathrm{BS}}$ into two sub-matrices, we have:

$$\boldsymbol{V}_{\mathrm{BS}} = \boldsymbol{A}\boldsymbol{B} \tag{24}.$$

The implementation block diagram is shown in Fig. 4. On the BS-side, K_{Down} original parallel transmit data streams $\boldsymbol{S}_{\mathrm{BS},t}$ are first passed through the conventional digital precoding matrix $\boldsymbol{B}$ to obtain f_D parallel data streams, and then through the SIC matrix $\boldsymbol{A}$ to obtain $N_{\mathrm{RF},t}$ parallel data streams, which are subsequently fed into the $N_{\mathrm{RF},t}$ transmit RF chains.

The first-stage matrix $\boldsymbol{B}$ is used for conventional digital precoding to suppress inter-user interference. At this point, the available degrees of freedom for conventional digital precoding are f_D. Matrix $\boldsymbol{B}$ can be derived using conventional digital precoding algorithms, such as Zero Forcing (ZF), MMSE, and singular value decomposition. In this paper, ZF is adopted for the design. By computing the pseudo-inverse of the channel matrix, signals in all directions other than the user direction is forced to zero, thus avoiding inter-user interference. Under the system architecture of this paper, the expression of matrix $\boldsymbol{B}$ is given as:

$$\boldsymbol{B} = \alpha_{\mathrm{equ}}\boldsymbol{H}_{\mathrm{equ}}^{\boldsymbol{H}}\left(\boldsymbol{H}_{\mathrm{equ}}\boldsymbol{H}_{\mathrm{equ}}^{\boldsymbol{H}}\right)^{-1} = \alpha_{\mathrm{equ}}\boldsymbol{W}_{\mathrm{ZF,equ}} \tag{25},$$

where $\alpha_{\mathrm{equ}} = \sqrt{\frac{K_1}{\mathrm{tr}(\boldsymbol{W}_{\mathrm{ZF,equ}}\boldsymbol{W}_{\mathrm{ZF,equ}}^{H})}}$ is the power control factor and K_1 is a constant; $\boldsymbol{H}_{\mathrm{equ}} = \boldsymbol{H}_{\mathrm{Down,equ}}\boldsymbol{A}$ is the equivalent channel. Therefore, when designing the first stage matrix $\boldsymbol{B}$, only the information of the equivalent channel $\boldsymbol{H}$ is required, and it is not necessary to obtain the information of the downlink channel $\boldsymbol{H}$ and matrix $\boldsymbol{A}$ separately.

The second-stage matrix $\boldsymbol{A}$ is used to minimize the total SI signal power while preserving the degrees of freedom f_D for the conventional digital precoding matrix $\boldsymbol{B}$. Therefore, the design objective of matrix $\boldsymbol{A}$ is to minimize the total SI signal power while preserving the required degrees of freedom f_D for the conventional digital precoding. Assuming that the equivalent SI channel $\boldsymbol{H}_{\mathrm{SI,equ}}$ is known, the design problem is formulated as follows:

$$\begin{aligned}\boldsymbol{A} = &\underset{\boldsymbol{A}}{\mathrm{argmin}} \left\| \boldsymbol{H}_{\mathrm{SI,equ}}\boldsymbol{A} \right\|_F^2 \\ &\mathrm{s.t.}\ \boldsymbol{A}^{\mathrm{H}}\boldsymbol{A} = \boldsymbol{E}_{f_D\times f_D}\end{aligned} \tag{26},$$

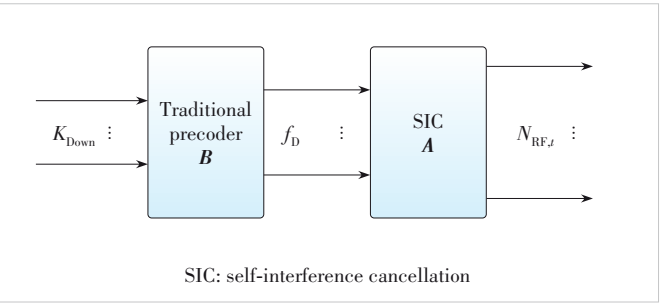

Figure 4. FD massive MIMO system with transmitting digital precoder

where $\left\| \boldsymbol{H}_{\mathrm{SI,equ}} \boldsymbol{A} \right\|_F^2$ is the total SI signal power and $\|\cdot\|_F^2$ is the square of the Frobenius parametrization; the constraint $\boldsymbol{A}^{\mathrm{H}}\boldsymbol{A} = \boldsymbol{E}_{f_D \times f_D}$ denotes that $\boldsymbol{A}$ has F orthogonal columns and is used to ensure that the required degrees of freedom f_D are preserved for conventional digital precoding. The solution to Eq. (26) is:

$$\boldsymbol{A} = \left[\boldsymbol{v}^{\left(N_{\mathrm{RF},t} - f_D + 1\right)} \quad \boldsymbol{v}^{\left(N_{\mathrm{RF},t} - f_D + 2\right)} \quad \cdots \quad \boldsymbol{v}^{\left(N_{\mathrm{RF},t}\right)} \right] \tag{27},$$

where $\mathrm{rank}\left(\boldsymbol{H}_{\mathrm{SI,equ}}\right) = r$ is assumed. $\sigma_1, \sigma_2, \cdots, \sigma_r$ are the r positive singular values of $\boldsymbol{H}_{\mathrm{SI,equ}}$. The singular value decomposition of matrix $\boldsymbol{H}_{\mathrm{SI,equ}}$ is $\boldsymbol{H}_{\mathrm{SI,equ}} = \boldsymbol{U}\boldsymbol{\Sigma}\boldsymbol{V}^H$, where $\boldsymbol{U} \in \boldsymbol{C}^{N_{\mathrm{RF},r} \times N_{\mathrm{RF},r}}$ and $\boldsymbol{V} \in \boldsymbol{C}^{N_{\mathrm{RF},t} \times N_{\mathrm{RF},t}}$ are both unitary matrices, $\boldsymbol{\Sigma} = \mathrm{diag}\left(\delta_1, \delta_2, \cdots, \delta_r, 0, 0, \cdots, 0\right) \in \boldsymbol{C}^{N_{\mathrm{RF},r} \times N_{\mathrm{RF},t}}$ is a diagonal matrix, and δ_i is a complex number satisfying $\left|\delta_i\right| = \sigma_i$; $\mathbf{v}^{(i)}$ is the i-th column of the matrix $\boldsymbol{V}$.

It can be seen that SI suppression matrix $\boldsymbol{A}$ is constructed by projecting onto the f_D right singular vectors corresponding to the f_D least singular values of the equivalent SI channel $\boldsymbol{H}_{\mathrm{SI,equ}}$. In essence, this process involves identifying the f_D-dimensional subspace in the original transmission space $\boldsymbol{C}^{N_{\mathrm{RF},t}}$ that minimizes the total SI received by the BS. Therefore, the greater the number of zero singular values of matrix $\boldsymbol{H}_{\mathrm{SI,equ}}$ (i.e., the smaller the rank r of the matrix $\boldsymbol{H}_{\mathrm{SI,equ}}$), the closer the f_D-dimensional subspace that minimizes the total SI received by the BS is to the zero space, and the better the SIC effect will be.

Next, the value of r is discussed for the proposed system architecture. Assume that $N_{\mathrm{RF}} = N_{\mathrm{RF},t} = N_{\mathrm{RF},r}$, $N = N_t = N_r$, $N^1 = N_t^k = N_r^k$, $N_{\mathrm{RF}}^1 = N_{\mathrm{RF},t}^k = N_{\mathrm{RF},r}^k$, $N_x = N_{t,x} = N_{r,x}$, and $N_y = N_{t,y} = N_{r,y}$. At this point, $\boldsymbol{C}_r = \boldsymbol{C}_t^{\mathrm{T}}$, and $\mathrm{rank}\left(\boldsymbol{C}_t\right) = N_{\mathrm{RF}}$. We let $\boldsymbol{C} = \boldsymbol{C}_t$ and $r_{\mathrm{SI}}^{11} = \mathrm{rank}\left(\boldsymbol{H}_{\mathrm{SI}}^{11}\right)$. First, we discuss the case of channel matrix $\boldsymbol{H}_{\mathrm{SI}}^{11}$ with a full rank, i.e., $r_{\mathrm{SI}}^{11} = N^1$. When $\boldsymbol{K} = \beta\boldsymbol{J}$ (where $\boldsymbol{J} \in \boldsymbol{C}^{N^1 \times N^1}$ is an all-ones matrix), the polarization isolation between each transceiver array element in different polarization directions is given by $P_{\mathrm{XPI,dB}} = -10\log 10\left(\beta\right)$ with $0 < \beta \leqslant 1$. Eq. (18) is equivalent to:

$$\boldsymbol{H}_{\mathrm{SI}} = \begin{bmatrix} \boldsymbol{H}_{\mathrm{SI}}^{11} & \beta\boldsymbol{H}_{\mathrm{SI}}^{11} \\ \beta\boldsymbol{H}_{\mathrm{SI}}^{11} & \boldsymbol{H}_{\mathrm{SI}}^{11} \end{bmatrix} \tag{28}.$$

The values of r are discussed for each of the three cases $0 < \beta < 1, \beta \to 0$ and $\beta = 1$.

When $0 < \beta < 1$, with chunk matrix multiplication, the equivalent self-interfering channel matrix expression is obtained as:

$$\boldsymbol{H}_{\mathrm{SI,equ}} = \begin{bmatrix} \boldsymbol{C}_{11}^{\mathrm{T}}\boldsymbol{H}_{\mathrm{SI}}^{11}\boldsymbol{C}_{11} & \beta\boldsymbol{C}_{11}^{\mathrm{T}}\boldsymbol{H}_{\mathrm{SI}}^{11}\boldsymbol{C}_{11} \\ \beta\boldsymbol{C}_{11}^{\mathrm{T}}\boldsymbol{H}_{\mathrm{SI}}^{11}\boldsymbol{C}_{11} & \boldsymbol{C}_{11}^{\mathrm{T}}\boldsymbol{H}_{\mathrm{SI}}^{11}\boldsymbol{C}_{11} \end{bmatrix} \tag{29},$$

where $\boldsymbol{C}_{11} \in \boldsymbol{C}^{N^1 \times N_{\mathrm{RF}}^1}$, and $\mathrm{rank}\left(\boldsymbol{C}_{11}\right) = N_{\mathrm{RF}}^1$. It can be obtained that:

$$r = 2 \times \mathrm{rank}\left(\boldsymbol{C}_{11}^{\mathrm{T}}\boldsymbol{H}_{\mathrm{SI}}^{11}\boldsymbol{C}_{11}\right) \leqslant N_{\mathrm{RF}} \tag{30}.$$

Similarly, when $\beta \to 0$,

$$r = 2 \times \mathrm{rank}\left(\boldsymbol{C}_{11}^{\mathrm{T}}\boldsymbol{H}_{\mathrm{SI}}^{11}\boldsymbol{C}_{11}\right) \leqslant N_{\mathrm{RF}} \tag{31}.$$

When $\beta = 1$,

$$r = \mathrm{rank}\left(\boldsymbol{C}_{11}^{\mathrm{T}}\boldsymbol{H}_{\mathrm{SI}}^{11}\boldsymbol{C}_{11}\right) \leqslant N_{\mathrm{RF}}^1 \tag{32}.$$

In summary,

$$r \leqslant \begin{cases} N_{\mathrm{RF}}, & 0 < \beta < 1 \\ N_{\mathrm{RF}}, & \beta \to 0 \\ N_{\mathrm{RF}}^1, & \beta = 1 \end{cases} \tag{33}.$$

For $0 < \beta < 1$, i.e., when the polarization isolation between the transmit and receive elements of different polarization directions is greater than 0 dB, the matrix $\boldsymbol{H}_{\mathrm{SI,equ}}$ may not have any zero singular values. That is to say, the f_D-dimensional subspace constructed by the f_D right singular vectors that minimize the total SI of BS reception is not completely close to the zero space, and the SIC effect is not good. When $\beta \to 0$, i.e., the polarization isolation between the transmit and receive elements of different polarization directions approaches infinity, the number of $\boldsymbol{H}_{\mathrm{SI,equ}}$ singular values of zero does not change significantly compared with $0 < \beta < 1$. In other words, the SIC performance does not improve significantly as polarization isolation increases. When $\beta = 1$, i.e., the polarization isolation between each transmit and receive array element with different polarization directions is 0 dB, it is evident from the structure of the transceiver URA that $N_{\mathrm{RF}} > N_{\mathrm{RF}}^1$. At this time, the number of $\boldsymbol{H}_{\mathrm{SI,equ}}$ singular values taking zero is at least $N_{\mathrm{RF}} - N_{\mathrm{RF}}^1 > 0$, which means that the f_D-dimensional subspace constructed by the f_D right singular vectors is closer to the zero space, and the SI cancellation effect is obviously enhanced. Therefore, the polarization isolation can be reduced to 0 dB to improve the SIC capability, if the polarization isolation between each transceiver array element in different polarization directions is the same.

According to the actual measurement of the engineering prototype, the polarization isolation between each transmit and receive array element with different polarization directions at different locations is not the same, indicating that the elements in the matrix $\boldsymbol{K}$ are not exactly equal. Therefore, the case of r at $\boldsymbol{K} \neq \beta\boldsymbol{J}$ is further discussed as follows. At this point, $\mathrm{rank}\left(\boldsymbol{K} \odot \boldsymbol{H}_{\mathrm{SI}}^{11}\right) \leqslant r_{\mathrm{SI}}^{11} = N^1$. For matrix $\boldsymbol{K} = \left(k_{ij}\right)_{N^1 \times N^1}$, we express it as:

$$\boldsymbol{K}=\left[\boldsymbol{k}_1,\quad \boldsymbol{k}_2,\quad \cdots\quad ,\boldsymbol{k}_{N^1}\right]=\left[\boldsymbol{g}_1^{\mathrm{T}},\quad \boldsymbol{g}_2^{\mathrm{T}},\quad \cdots\quad ,\boldsymbol{g}_{N^1}^{\mathrm{T}}\right]^{\mathrm{T}} \tag{34}$$

where $\boldsymbol{k}_j \in \boldsymbol{C}^{N^1\times 1}, j=1,2,\cdots,N^1$, and $\boldsymbol{g}_i \in \mathbf{C}^{1\times N^1}, i=1,2,\cdots,N^1$. We let $\boldsymbol{H}_{\mathrm{SI}}=\left(h_{i,j}\right)_{N\times N}$. At this point, the expression of the equivalent SI channel $\boldsymbol{H}_{\mathrm{SI,equ}}$ is:

$$\boldsymbol{H}_{\mathrm{SI,equ}}=\begin{bmatrix}\boldsymbol{H}_{\mathrm{SI,equ}}^{11} & \boldsymbol{H}_{\mathrm{SI,equ}}^{12}\\ \boldsymbol{H}_{\mathrm{SI,equ}}^{12} & \boldsymbol{H}_{\mathrm{SI,equ}}^{11}\end{bmatrix}==\begin{bmatrix}\boldsymbol{C}_{11}^{\mathrm{T}}\boldsymbol{H}_{\mathrm{SI}}^{11}\boldsymbol{C}_{11} & \boldsymbol{C}_{11}^{\mathrm{T}}\left(\boldsymbol{K}\odot\boldsymbol{H}_{\mathrm{SI}}^{11}\right)\boldsymbol{C}_{11}\\ \boldsymbol{C}_{11}^{\mathrm{T}}\left(\boldsymbol{K}\odot\boldsymbol{H}_{\mathrm{SI}}^{11}\right)\boldsymbol{C}_{11} & \boldsymbol{C}_{11}^{\mathrm{T}}\boldsymbol{H}_{\mathrm{SI}}^{11}\boldsymbol{C}_{11}\end{bmatrix} \tag{35}$$

where $\mathrm{rank}\left(\boldsymbol{H}_{\mathrm{SI,equ}}^{11}\right)\leqslant N_{\mathrm{RF}}^1$, $\mathrm{rank}\left(\boldsymbol{H}_{\mathrm{SI,equ}}^{12}\right)\leqslant \begin{cases}\mathrm{rank}\left(\boldsymbol{K}\odot\boldsymbol{H}_{\mathrm{SI}}^{11}\right) & \mathrm{rank}\left(\boldsymbol{K}\odot\boldsymbol{H}_{\mathrm{SI}}^{11}\right)<N_{\mathrm{RF}}^1\\ N_{\mathrm{RF}}^1 & \mathrm{rank}\left(\boldsymbol{K}\odot\boldsymbol{H}_{\mathrm{SI}}^{11}\right)\geqslant N_{\mathrm{RF}}^1\end{cases}$. Denote the j-th column of $\boldsymbol{H}_{\mathrm{SI,equ}}^{11}$ and $\boldsymbol{H}_{\mathrm{SI,equ}}^{12}$ as $\boldsymbol{h}_{\mathrm{SI,equ},j}^{11}$ and $\boldsymbol{h}_{\mathrm{SI,equ},j}^{12}$ respectively, where the elements of $\boldsymbol{h}_{\mathrm{SI,equ},j}^{11}$ and $\boldsymbol{h}_{\mathrm{SI,equ},j}^{12}$ are $\sum_{k,l=0,N_y,2N_y} h_{i+k,j+l}$, and $\sum_{k,l=0,N_y,2N_y} k_{i+k,j+l}h_{i+k,j+l}$ $(i=1,2,\cdots,N_y,3N_y+1,3N_y+2,\cdots,4N_y,\cdots,N^1;j=1,2,\cdots,N_{\mathrm{RF}}^1)$.

To minimize the rank r of the matrix $\boldsymbol{H}_{\mathrm{SI,equ}}$, it is necessary that the j-th column of $\boldsymbol{H}_{\mathrm{SI,equ}}^{12}$ in Eq. (35) is equal to the j-th column of $\boldsymbol{H}_{\mathrm{SI,equ}}^{11}$, i.e., the following condition must be satisfied.

$$\sum_{k,l=0,N_y,2N_y} k_{i+k,j+l}h_{i+k,j+l}=\sum_{k,l=0,N_y,2N_y} h_{i+k,j+l} \tag{36}$$

which can be rewritten as:

$$k_{i+k,j+l}=1 \tag{37}$$

where $i=1,2,\cdots,N_y,3N_y+1,3N_y+2,\cdots,4N_y,\cdots,N^1$, $k,l=0,N_y,2N_y$. Eq. (37) is equivalent to:

$$\boldsymbol{k}_j=\boldsymbol{k}_{j+N_y}=\boldsymbol{k}_{j+2N_y}=\left[1,\quad 1,\quad \cdots\quad ,1\right]^{\mathrm{T}} \tag{38}$$

In other words, the polarization isolation between each transmit and receive array element with different polarization directions at the corresponding position of Eq. (38) is close to 0 dB. According to the structure of the transmit-receive URA, the polarization isolation between the transmit array element connected to the j-th transmit RF channel and all the receive array elements is 0 dB under this condition. Similarly, r can be reduced when the i-th row of $\boldsymbol{H}_{\mathrm{SI,equ}}^{12}$ in Eq. (35) is equal to that of $\boldsymbol{H}_{\mathrm{SI,equ}}^{11}$, i.e.,

$$\boldsymbol{g}_i=\boldsymbol{g}_{i+N_y}=\boldsymbol{g}_{i+2N_y}=\left[1,\quad 1,\quad \cdots\quad ,1\right] \tag{39}$$

At this point, the polarization isolation between the receive array connected to the i-th receive RF channel and all transmit arrays is 0 dB. Note that W is the set of column numbers of the column vector $\boldsymbol{k}_j$ satisfying Eq. (38), P is the set of row numbers of the row vector $\boldsymbol{g}_i$ satisfying Eq. (39), $w=|W|$ is the number of elements in the set, and $p=|P|$ is the number of elements in the set P. We have:

$$r=\mathrm{rank}\left(\left[\boldsymbol{H}_{\mathrm{SI,equ}}^{11}\quad \boldsymbol{H}_{\mathrm{SI,equ}}^{12}\right]\right)-w-p \tag{40}$$

where

$$\mathrm{rank}\left(\left[\boldsymbol{H}_{\mathrm{SI,equ}}^{11}\quad \boldsymbol{H}_{\mathrm{SI,equ}}^{12}\right]\right)\leqslant \begin{cases}N_{\mathrm{RF}}^1+\mathrm{rank}\left(\boldsymbol{K}\odot\boldsymbol{H}_{\mathrm{SI}}^{11}\right) & \mathrm{rank}\left(\boldsymbol{K}\odot\boldsymbol{H}_{\mathrm{SI}}^{11}\right)<N_{\mathrm{RF}}^1\\ N_{\mathrm{RF}} & \mathrm{rank}\left(\boldsymbol{K}\odot\boldsymbol{H}_{\mathrm{SI}}^{11}\right)\geqslant N_{\mathrm{RF}}^1\end{cases} \tag{41}$$

At this point, r is related to the rank of matrix $\boldsymbol{K}\odot\boldsymbol{H}_{\mathrm{SI}}^{11}$ and the number of unit row (or column) vectors in matrix $\boldsymbol{K}$. Therefore, in practical engineering implementations, $\boldsymbol{K}$ can be designed so that either the rank of $\boldsymbol{K}\odot\boldsymbol{H}_{\mathrm{SI}}^{11}$ is less than N_{RF}^1, or the polarization isolation between the transmit (or receive) array elements connected to as many transmit (or receive) RF channels as possible and all the corresponding receive (or transmit) array elements is 0 dB, in order to achieve better SIC performance. It should be noted that when using the $\boldsymbol{K}$ method, if the rank of $\boldsymbol{K}\odot\boldsymbol{H}_{\mathrm{SI}}^{11}$ is only reduced but remains greater than N_{RF}^1, it will not yield a significant improvement in SIC capability.

In practice, the antenna array placement of massive MIMO does not always result in completely uncorrelated and independent channels. In such cases, channel matrix $\boldsymbol{H}_{\mathrm{SI}}^{11}$ is non-full rank, i.e., $r_{\mathrm{SI}}^{11}<N^1$. The corresponding value of rank r when $r_{\mathrm{SI}}^{11}<N^1$ is analyzed below. When $\boldsymbol{K}=\beta\boldsymbol{J}$, the same three cases are discussed in terms of $0<\beta<1$, $\beta\to 0$ and $\beta=1$.

When $r_{\mathrm{SI}}^{11}<N_{\mathrm{RF}}^1$,

$$\mathrm{rank}\left(\boldsymbol{H}_{\mathrm{SI,equ}}\right)\leqslant\begin{cases}2r_{\mathrm{SI}}^{11}, & 0<\beta<1\\ 2r_{\mathrm{SI}}^{11}, & \beta\to 0\\ r_{\mathrm{SI}}^{11}, & \beta=1\end{cases} \tag{42}$$

When $r_{\mathrm{SI}}^{11}\geqslant N_{\mathrm{RF}}^1$,

$$\mathrm{rank}\left(\boldsymbol{H}_{\mathrm{SI,equ}}\right)\leqslant\begin{cases}N_{\mathrm{RF}}, & 0<\beta<1\\ N_{\mathrm{RF}}, & \beta\to 0\\ N_{\mathrm{RF}}^1, & \beta=1\end{cases} \tag{43}$$

Therefore, when $N_{\mathrm{RF}}^1\leqslant r_{\mathrm{SI}}^{11}<N^1$, r does not change much compared with the case where $\boldsymbol{H}_{\mathrm{SI}}^{11}$ is full rank. When $r_{\mathrm{SI}}^{11}<N_{\mathrm{RF}}^1$, r decreases, and at this time, the number of zero singular values of $\boldsymbol{H}_{\mathrm{SI,equ}}$ is at least $N_{\mathrm{RF}}-2r_{\mathrm{SI}}^{11}$ $(0<N_{\mathrm{RF}}-2r_{\mathrm{SI}}^{11}<N_{\mathrm{RF}})$. Thus, the f_D-dimensional subspace constructed by f_D

right singular vectors is closer to the zero space, and the SI canceling performance is significantly enhanced. Consequently, in practical engineering implementation, to enhance SIC performance by changing the rank r_{SI}^{11} of $\boldsymbol{H}_{\mathrm{SI}}^{11}$, r_{SI}^{11} should be reduced to at least less than the number of transmit or receive RF channels connected to the antenna array elements with the same polarization direction.

When $\boldsymbol{K} \neq \beta \boldsymbol{J}$, it can be obtained similarly that

$$r = \mathrm{rank}\left(\left[\boldsymbol{H}_{\mathrm{SI},\mathrm{equ}}^{11} \quad \boldsymbol{H}_{\mathrm{SI},\mathrm{equ}}^{12}\right]\right) - w - p \tag{44},$$

where,

$$\mathrm{rank}\left(\left[\boldsymbol{H}_{\mathrm{SI},\mathrm{equ}}^{11} \quad \boldsymbol{H}_{\mathrm{SI},\mathrm{equ}}^{12}\right]\right) \leqslant \begin{cases} r_{\mathrm{SI}}^{11} + \mathrm{rank}\left(\boldsymbol{K} \odot \boldsymbol{H}_{\mathrm{SI}}^{11}\right), & r_{\mathrm{SI}}^{11} < N_{\mathrm{RF}}^{1} \\ N_{\mathrm{RF}}^{1} + \mathrm{rank}\left(\boldsymbol{K} \odot \boldsymbol{H}_{\mathrm{SI}}^{11}\right), & \mathrm{rank}\left(\boldsymbol{K} \odot \boldsymbol{H}_{\mathrm{SI}}^{11}\right) < N_{\mathrm{RF}}^{1} \leqslant r_{\mathrm{SI}}^{11} \\ N_{\mathrm{RF}}, & \mathrm{rank}\left(\boldsymbol{K} \odot \boldsymbol{H}_{\mathrm{SI}}^{11}\right) \geqslant N_{\mathrm{RF}}^{1} \end{cases} \tag{45}.$$

Thus, when $\boldsymbol{K} \neq \beta \boldsymbol{J}$, the rank r is related not only to the rank of $\boldsymbol{K} \odot \boldsymbol{H}_{\mathrm{SI}}^{11}$ and the number of unit row (or column) vectors in $\boldsymbol{K}$, but also to the rank r_{SI}^{11} of $\boldsymbol{H}_{\mathrm{SI}}^{11}$. Accordingly, in practical engineering implementations, to enhance the SI cancellation capability, in addition to designing $\boldsymbol{K}$ to minimize the rank of $\boldsymbol{K} \odot \boldsymbol{H}_{\mathrm{SI}}^{11}$ (i.e., ensuring it is less than N_{RF}^{1}), or maximizing the number of transmit (receive) array elements connected to transmit (receive) RF chains for which the polarization isolation with all corresponding receive (transmit) array elements is 0 dB, r_{SI}^{11} can also be reduced to less than the number of transmit or receive RF channels connected to the antenna array elements with the same polarization direction .

In this paper, we also consider whether the SIC performance can be further enhanced by changing the array placement. The transmitting and receiving URAs placed vertically along the x-axis in Fig. 3 are reconfigured to a diagonal placement along the same axis. The equivalent SI channel matrix $\boldsymbol{H}_{\mathrm{SI},\mathrm{equ}}$ obtained at this point is the same as that in Eq. (38). This is because using different array placements only changes the values of the elements of the sub-matrix $\boldsymbol{H}_{\mathrm{SI}}^{11}$, but the transmit or receive array elements of both polarization directions are still in the same position. Thus the form of $\boldsymbol{H}_{\mathrm{SI},\mathrm{equ}}$ will not change. Therefore, the rank r_{SI}^{11} of the channel matrix $\boldsymbol{H}_{\mathrm{SI}}^{11}$ can be minimized by changing the array placement, so that the SIC performance can be improved.

According to the above analysis, the SI cancellation effect can be enhanced from three perspectives: 1) by designing matrix $\boldsymbol{K}$ so that the rank of $\boldsymbol{K} \odot \boldsymbol{H}_{\mathrm{SI}}^{11}$ is less than the number of transmit or receive RF channels connected to the antennas with the same polarization direction; 2) by making the polarization isolation between the transmit (receive) array elements connected to the same transmit (receive) RF channel and all receive (transmit) array elements 0 dB; 3) by reducing the rank r_{SI}^{11} of $\boldsymbol{H}_{\mathrm{SI}}^{11}$ to be smaller than the number of transmit or receive RF channels connected to antennas with the same polarization direction, such as changing the array placement and widening the transceiver URA spacing. Although the channel is modeled as narrowband in the above analysis, beamforming is also applicable to the wideband channel model. This is because beamforming targets frequency-domain data and is implemented at the subcarrier level.

4 Illustrative Results

In this section, the SoftNull algorithm performance for the proposed system is evaluated through simulations from the sum rate and SIC. The downlink achievable rate can be given by:

$$R_{\mathrm{DL}} = \log_2\left|\boldsymbol{I}_{K_{\mathrm{Down}}} + \boldsymbol{R}_{\mathrm{UE}}^{-1}\boldsymbol{W}_{\mathrm{DL}}\right| \tag{46},$$

where $\boldsymbol{R}_{\mathrm{UE}} = \mathrm{E}\left\{\boldsymbol{n}_{\mathrm{UE}}\boldsymbol{n}_{\mathrm{UE}}^{H}\right\}$, and $\mathrm{E}\{\cdot\}$ denotes the statistical expectation. $\boldsymbol{W}_{\mathrm{DL}}$ represents the received covariance matrices of the downlink channel, which is defined as:

$$\boldsymbol{W}_{\mathrm{DL}} = \boldsymbol{H}_{\mathrm{Down},\mathrm{equ}}\boldsymbol{G}_{\mathrm{BS}}\boldsymbol{H}_{\mathrm{Down},\mathrm{equ}}^{H} \tag{47},$$

where $\boldsymbol{G}_{\mathrm{BS}} = \boldsymbol{F}^{H}\boldsymbol{V}_{\mathrm{BS}}\mathrm{E}\left\{\boldsymbol{S}_{\mathrm{BS},t}\boldsymbol{S}_{\mathrm{BS},t}^{H}\right\}\boldsymbol{V}_{\mathrm{BS}}^{H}\boldsymbol{F}$. Similarly, the uplink (UL) rate is expressed as:

$$R_{\mathrm{UL}} = \log_2\left|\boldsymbol{I}_{K_{\mathrm{Up}}} + \left(\boldsymbol{R}_{\mathrm{BS}} + \boldsymbol{Q}_{\mathrm{BS}}\right)^{-1}\boldsymbol{W}_{\mathrm{UL}}\right| \tag{48},$$

where $\boldsymbol{R}_{\mathrm{BS}} = \boldsymbol{U}_{\mathrm{BS}}\boldsymbol{F}\mathrm{E}\left\{\boldsymbol{n}_{\mathrm{BS}}\boldsymbol{n}_{\mathrm{BS}}^{H}\right\}\boldsymbol{F}^{H}\boldsymbol{U}_{\mathrm{BS}}^{H}$ denotes the power of received noise, $\boldsymbol{Q}_{\mathrm{BS}}$ and $\boldsymbol{W}_{\mathrm{UL}}$ are the downlink receive covariance matrices for the SI and intended signal on the BS side, respectively, defined as:

$$\boldsymbol{Q}_{\mathrm{BS}} = \boldsymbol{U}_{\mathrm{BS}}\boldsymbol{F}\boldsymbol{H}_{\mathrm{SI},\mathrm{equ}}\boldsymbol{G}_{\mathrm{BS}}\boldsymbol{H}_{\mathrm{SI},\mathrm{equ}}^{H}\boldsymbol{F}^{H}\boldsymbol{U}_{\mathrm{BS}}^{H} \tag{49},$$

$$\boldsymbol{W}_{\mathrm{UL}} = \boldsymbol{U}_{\mathrm{BS}}\boldsymbol{F}\boldsymbol{H}_{\mathrm{Up},\mathrm{equ}}\boldsymbol{G}_{\mathrm{UE}}\boldsymbol{H}_{\mathrm{Up},\mathrm{equ}}^{H}\boldsymbol{F}^{H}\boldsymbol{U}_{\mathrm{BS}}^{H} \tag{50},$$

where $\boldsymbol{G}_{\mathrm{UE}} = \mathrm{E}\left\{\boldsymbol{x}_{\mathrm{UE},t}\boldsymbol{x}_{\mathrm{UE},t}^{H}\right\}$. Accordingly, the achievable rate can be written as:

$$R_{\mathrm{sum}} = R_{\mathrm{DL}} + R_{\mathrm{UL}} = \log_2\left|\boldsymbol{I}_{K_{\mathrm{Down}}} + \boldsymbol{R}_{\mathrm{UE}}^{-1}\boldsymbol{W}_{\mathrm{DL}}\right| + \log_2\left|\boldsymbol{I}_{K_{\mathrm{Up}}} + \left(\boldsymbol{R}_{\mathrm{BS}} + \boldsymbol{Q}_{\mathrm{BS}}\right)^{-1}\boldsymbol{W}_{\mathrm{UL}}\right| \tag{51}.$$

The parameters are summarized in Table 1, where λ is the wavelength. It is assumed that the NLOS path between each transmit and receive antenna pair is reflected by the point o_{wall}.

In Fig. 5, we investigate the SIC of each receiving RF channel versus the degrees of freedom f_D reserved for traditional digital precoding under the SoftNull scheme. We assume that the antenna isolation is 0 dB and the URA spacing is 0.2 m, which is 1.7 times the wavelength.

As can be observed, a decrease in f_D corresponds to an in-

Table 1. Simulation parameters of full-duplex massive MIMO system

Parameter	Value
Bandwidth	100 MHz
Center frequency	2.595 GHz
Transmit power of base station	30 dBm
Transmit power of user	30 dBm
Number of base station antennas	$N_t = N_r = 6 \times 8 \times 2 = 96$
Number of base station RF channels	$N_{RF,t} = N_{RF,r} = 32$
Number of uplink users	$K_{Up} = 2 \times 4 = 8$
Number of downlink users	$K_{Down} = 2 \times 4 = 8$
Antenna spacing along x-axis	$d_{t,x} = d_{r,x} = 0.67\lambda$
Antenna spacing along y-axis	$d_{r,y} = d_{t,y} = 0.5\lambda$
URAs spacing	$d_1 = 0.5\lambda$
User spacing along x-axis	$d_{Up,x} = d_{Down,x} = 2.679\,5$ m
User spacing along y-axis	$d_{Up,y} = d_{Down,y} = 2.679\,5$ m
Cross-polarization isolation	$P_{XPI,dB} = 25$ dB
Path loss factor	$\eta = 2.92$
Number of uplink channel multipaths	$C_{Up} = 1, L_{Up,c} = 1, L_{Up} = 1$
Number of downlink channel multipaths	$C_{Down} = 1, L_{Down,c} = 1, L_{Down} = 1$
Number of SI channel multipaths	$C_{SI} = 1, L_{SI,c} = 1, L_{SI} = 1$

URA: Uniform rectangular array

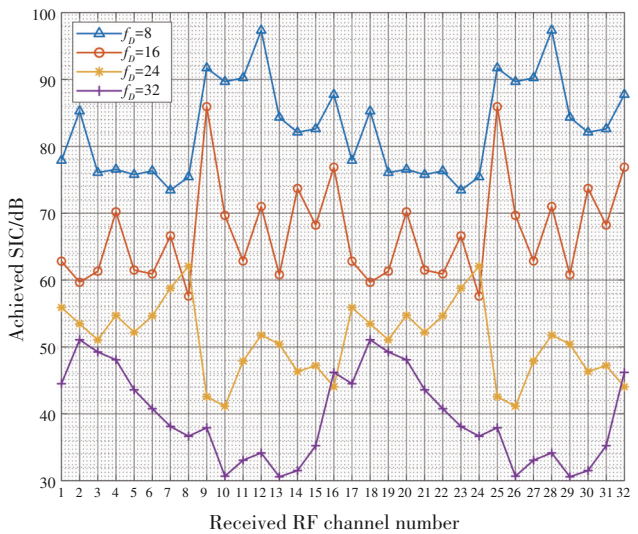

RF: radio frequenc SIC: self-interference cancellation

Figure 5. Impact of f_D on SIC in received RF channels

crease in the SIC performance for each receive RF chain. This is because a reduction in the degrees of freedom assigned to traditional digital precoding invariably increases the degrees of freedom available for SIC, resulting in enhanced SIC performance. Additionally, the SIC performance of different receive RF channels fluctuates to varying degrees, since the design goal of the SI suppression matrix is to minimize the total SI signal power rather than the SI signal power of each receiving RF

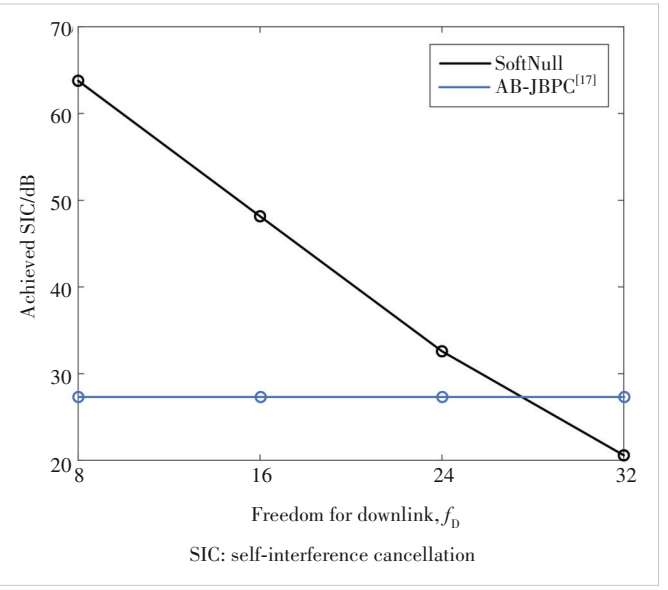

SIC: self-interference cancellation

Figure 6. Impact of f_D on total SIC

channel. In Fig. 6, we further investigate f_D versus the total SIC.

However, when we utilize the SoftNull scheme in the proposed system architecture, the total SI channel power can be suppressed by up to 64 dB as shown in Fig. 6, including a path loss of 21 dB. The total SIC performance exhibits an increasing trend with a decrease in the degrees of freedom used for downlinks, similar to the SIC for each receive RF channel. Compared with AB-JHPC[17] with only transmit beamforming, the proposed SoftNull scheme achieves higher SIC performance when the reserved degrees of freedom are less than 24.

Accordingly, SoftNull can achieve different SI suppression effects by changing the value of f_D within the proposed system architecture. However, the degrees of freedom available for

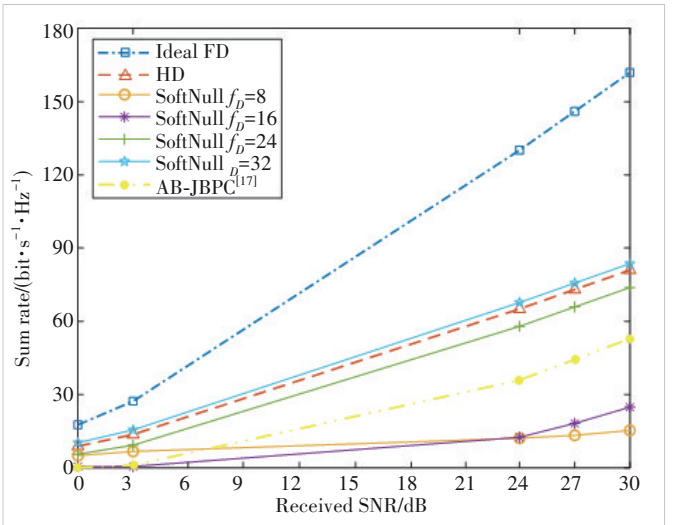

FD: full-duplex HD: half-duplex SNR: signal-to-noise ratio

Figure 7. Impact of f_D on sum rate

downlink traditional beamforming also change. We further investigate the impact of f_D adjustment on the sum rate. Fig. 7 plots the relationship between f_D and the sum rate under SoftNull, along with a performance comparison of HD, ideal FD, and AB-JHPC with only transmit beamforming.

It can be observed that the achievable sum rate increases with the increase of f_D. The maximum sum rate is improved by 16% compared with that of HD, when all available degrees of freedom are used for traditional digital precoding. However, the achieved SIC is only 21 dB from path loss, showing that the SI power on the UL reception is higher than the received desired signal power. It not only causes RF saturation of the receiver but also induces harm to the receiver hardware. Thus, we should choose a reasonable value of f_D to balance the trade-off between the achieved SIC and the sum rate. In this way, a higher sum rate can be achieved without saturating the receive RF channels on the BS side.

In addition, the achievable sum rate is much smaller than that of the ideal FD. This is because reducing f_D can enhance SIC performance to improve the signal-to-interference plus noise ratio (SINR) and achieve a higher uplink rate, while it has a negative impact on the downlink rate. The uplink rate gain achieved by enhancing SIC performance is unable to compensate for the downlink rate loss. Thus, even when a certain SIC is achieved, the sum rate is low.

To improve the performance of the proposed full-duplex mas-

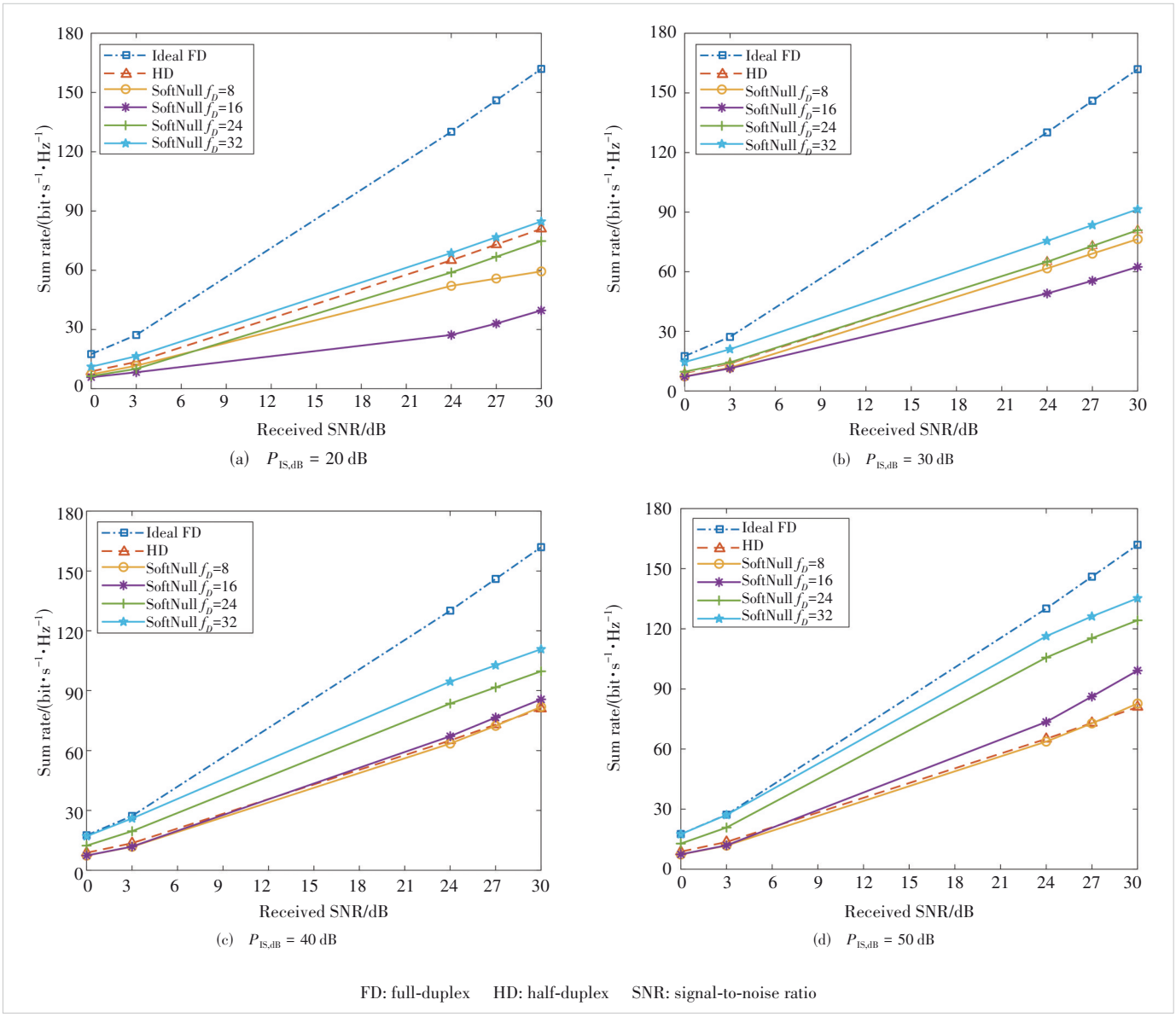

FD: full-duplex HD: half-duplex SNR: signal-to-noise ratio

Figure 8. Impact of antenna isolation on sum rate

sive MIMO system with large antenna arrays, antenna isolation is used to further suppress the received SI, thereby enabling a higher sum rate while enhancing the total SIC performance. Fig. 8 depicts the sum rate with different antenna isolation.

Increasing antenna isolation further reduces the received SI signal, so that the uplink rate is improved. When more antenna isolation is utilized, the sum rate increases under different f_D. The received SI power is much smaller than the received intended signal power. And the achieved sum rate is higher than that of HD and approaches the ideal FD, when the antenna isolation is increased to 50 dB and f_D = 32. The results with the sum rate are increased by 26.7% compared with those using only the SoftNull algorithm, and 67% to 100% higher than the HD.

As an increase in antenna isolation causes a corresponding decrease in the received SI power, the received UL SINR is infinitely close to the received SNR. Thus, the sum rate under SoftNull cannot increase linearly with the increase of antenna isolation. The lower the received SNR, the smaller the total SIC required to achieve the same rate situation.

The SIC performance and the sum rate can also be further enhanced by increasing the spacing between the transmit and receive URAs. Fig. 9 depicts the sum rate with different antenna isolation when d_1 is increased to 5λ.

As can be observed, an increase in the distance between transmit and receive URAs under the same antenna isolation corresponds to an increase in the sum rate compared with that in Figs. 8c and 8d. When the antenna isolation is 50 dB, the sum rate can be increased by up to 54%, which is 90% to 100% higher than that of HD. The f_D-dimensional subspace found under the same available degrees of freedom and antenna isolation is closer to the null space by increasing the distance of the transceiver URAs, which reduces the rank r_{SI}^{11}. Thus, the received UL SINR and the sum rate performance are improved. It is necessary to reasonably select f_D, antenna isolation, and d_1 with the requirements when using SoftNull to achieve SI elimination under the proposed system architecture, so as to improve the sum rate while achieving the required SIC.

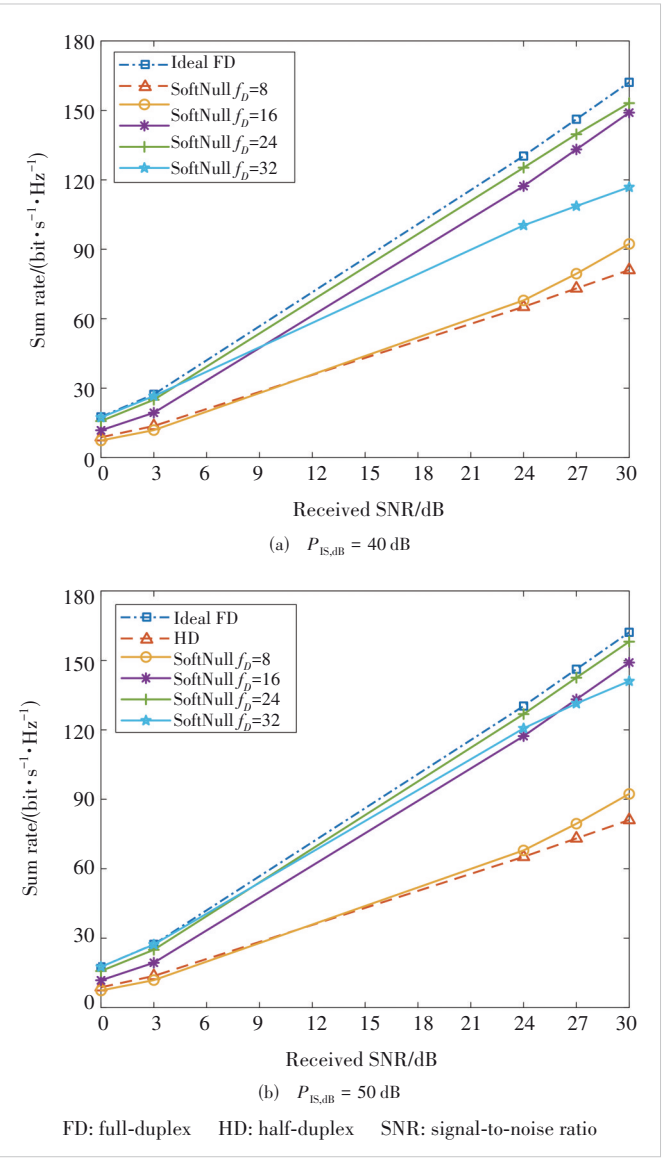

Figure 9. Impact of antenna isolation on sum rate with transceiver uniform rectangular array spacing of 5λ

5 Conclusions

In this paper, a structure for the FD massive MIMO communication system with multi-stream transmission, where one transmit or receive RF channel is connected with three transmitting or receiving antennas in the same polarization direction, is proposed. This structure greatly reduces power dissipation and cost. To avoid LNA saturation caused by SI signals, the SoftNull algorithm based on transmit digital precoding is proposed. In addition, the method of enhancing the SIC under the algorithm is analyzed. We consider the method of antenna isolation and increasing the distance between receive and transmit URAs to improve system performance. Simulation results show that the SoftNull algorithm can achieve SI suppression in the architecture. Moreover, the method of joint antenna isolation and increasing the distance between the transmit-receiver URAs can further enhance system performance.

References

[1] BOCCARDI F, HEATH R W, LOZANO A, et al. Five disruptive technology directions for 5G [J]. IEEE communications magazine, 2014, 52(2): 74 – 80. DOI: 10.1109/MCOM.2014.6736746
[2] AGIWAL M, ROY A, SAXENA N. Next generation 5G wireless networks: a comprehensive survey [J]. IEEE communications surveys & tutorials, 2016, 18(3): 1617 – 1655. DOI: 10.1109/COMST.2016.2532458
[3] HU Y F, WANG D M, LIANG C L, et al. Massive random access in cell-free massive MIMO system [J]. ZTE technology journal, 2024, 30(1): 26 – 32. DOI: 10.12142/ZTETJ.202401006

[4] HAN Y, ZHANG J Y, JIN S. U6G extra-large scale MIMO technology [J]. ZTE technology journal, 2024, 30(3): 67 – 71. DOI: 10.12142/ZTETJ.202403011
[5] ZHANG Z S, CHAI X M, LONG K P, et al. Full-duplex techniques for 5G networks: SI cancellation, protocol design, and relay selection [J]. IEEE communications magazine, 2015, 53(5): 128 – 137. DOI: 10.1109/MCOM.2015.7105651
[6] AGHABABAEETAFRESHI M, KORPI D, KOSKELA M, et al. Software defined radio implementation of a digital SI cancellation method for in-band full-duplex radio using mobile processors [J]. Journal of signal processing systems, 2018, 90(10): 1297 – 1309. DOI: 10.1007/s11265-017-1312-0
[7] NGO H Q, LARSSON E G, MARZETTA T L. Energy and spectral efficiency of very large multiuser MIMO systems [J]. IEEE transactions on communications, 2013, 61(4): 1436 – 1449. DOI: 10.1109/TCOMM.2013.020413.110848
[8] HUANG Y M, HE S W, WANG J H, et al. Spectral and energy efficiency tradeoff for massive MIMO [J]. IEEE transactions on vehicular technology, 2018, 67(8): 6991 – 7002. DOI: 10.1109/TVT.2018.2824311
[9] TRAN T X, TEH K C. Spectral and energy efficiency analysis for SLNR precoding in massive MIMO systems with imperfect CSI [J]. IEEE transactions on wireless communications, 2018, 17(6): 4017 – 4027. DOI: 10.1109/TWC.2018.2819184
[10] PIRZADEH H, SWINDLEHURST A L. Spectral efficiency of mixed-ADC massive MIMO [J]. IEEE transactions on signal processing, 2018, 66(13): 3599 – 3613. DOI: 10.1109/TSP.2018.2833807
[11] ZHANG X, ZHONG L, SABHARWAL A. Directional training for FDD massive MIMO [J]. IEEE transactions on wireless communications, 2018, 17(8): 5183 – 5197. DOI: 10.1109/TWC.2018.2838600
[12] YIN B, WU M, STUDER C, et al. Full-duplex in large-scale wireless systems [C]//Asilomar Conference on Signals, Systems and Computers. IEEE, 2013: 1623 – 1627. DOI: 10.1109/ACSSC.2013.6810573
[13] NGO H Q, SURAWEERA H A, MATTHAIOU M, et al. Multipair full-duplex relaying with massive arrays and linear processing [J]. IEEE journal on selected areas in communications, 2014, 32(9): 1721 – 1737. DOI: 10.1109/JSAC.2014.2330091
[14] GOLDSMITH A. Wireless Communications [M]. Cambridge, UK: Cambridge University Press, 2005
[15] AHMED E, ELTAWIL A M. All-digital SI cancellation technique for full-duplex systems [J]. IEEE transactions on wireless communications, 2015, 14(7): 3519 – 3532. DOI: 10.1109/TWC.2015.2407876
[16] LE A T, TRAN L C, HUANG X J, et al. Beam-based analog SI cancellation in full-duplex MIMO systems [J]. IEEE transactions on wireless communications, 2020, 19(4): 2460 – 2471. DOI: 10.1109/TWC.2020.2965441
[17] ALEXANDROPOULOS G C, DUARTE M. Joint design of multi-tap analog cancellation and digital beamforming for reduced complexity full duplex MIMO systems [C]//Proceedings of IEEE International Conference on Communications (ICC). IEEE, 2017: 1 – 7. DOI: 10.1109/ICC.2017.7997175
[18] IIMORI H, THADEU FREITAS DE ABREU G. Two-way full-duplex MIMO with hybrid TX-RX MSE minimization and interference cancellation [C]//IEEE 19th International Workshop on Signal Processing Advances in Wireless Communications (SPAWC). IEEE, 2018: 1 – 5. DOI: 10.1109/SPAWC.2018.8445776
[19] KOC A, LE-NGOC T. Full-duplex mmWave massive MIMO systems: a joint hybrid precoding/combining and SI cancellation design [J]. IEEE open journal of the communications society, 2021, 2: 754 – 774. DOI: 10.1109/OJCOMS.2021.3069672
[20] SATYANARAYANA K, EL-HAJJAR M, KUO P H, et al. Hybrid beamforming design for full-duplex millimeter wave communication [J]. IEEE transactions on vehicular technology, 2019, 68(2): 1394 – 1404. DOI: 10.1109/TVT.2018.2884049
[21] EVERETT E, SHEPARD C, ZHONG L, et al. SoftNull: many-antenna full-duplex wireless via digital beamforming [J]. IEEE transactions on wireless communications, 2016, 15(12): 8077 – 8092. DOI: 10.1109/TWC.2016.2612625

Biographies

ZHANG Boyu received his bachelor's degree in electronic information engineering from University of Electronic Science and Technology of China (UESTC) in 2022. He is currently working towards a master's degree in communication and information engineering at UESTC. His research interests include wireless communication and full duplex for massive MIMO systems.

ZHANG Ling received her master's degree from University of Electronic Science and Technology of China (UESTC) in 2023. She is currently a chip and device design engineer. Her research interests include wireless communications, massive MIMO systems, chip development.

LI Zijing received her master's degree in electronic information engineering from University of Electronic Science and Technology of China (UESTC) in 2023. She is currently working towards a PhD degree in communication and information engineering at UESTC. Her research interests include SI suppression and integrated communication and sensing for massive MIMO systems.

SHEN Ying (shenying@uestc.edu.cn) received his PhD degree in communication and information systems from University of Electronic Science and Technology of China (UESTC) in 2009. He is currently working at the National Key Laboratory of Wireless Communications, UESTC. His research interests include full-duplex, MIMO, and broadcasting systems.